Eur. Phys. J. AP **7**, 25–32 (1999)

THE EUROPEAN PHYSICAL JOURNAL APPLIED PHYSICS

Application of crystal orientation mapping to local orientation perturbations

R.K. Davies[a] and V. Randle

Department of Materials Engineering, University of Wales Swansea, Singleton Park, Swansea SA2 8PP, UK

Received: 28 July 1998 / Revised: 18 December 1998 / Accepted: 6 April 1999

Abstract. Crystal Orientation Mapping (COM) is a new state-of-the-art technique for making spatially specific orientation measurements based on the automatic analysis of electron backscatter diffraction patterns. The main aim of the work reported is to demonstrate the quantitative application of COM for characterising local orientation perturbations in the vicinity of triple junctions in an Al-3wt%Mg alloy deformed 5% in tension. First, the hardware configuration of the EBSD system is described and the optimum microscope operating conditions for setting up a COM are determined by measuring the spatial resolution of EBSD patterns in pure Al and Ni specimens. For this particular investigation, an accelerating voltage of 20 kV was found to be optimum for mapping, resulting in spatial resolutions of 0.51 μm and 0.42 μm for Al and Ni respectively. Secondly, to provide a visual representation of local orientation perturbations in the vicinity of a triple junction, a COM and pattern quality map are presented. The "raw" orientation data extracted from the COM was quantified using several different post-processing methods. The methodology associated with each is discussed and comparisons of the pattern of orientation perturbations are made using the same "raw" data set.

PACS. 61.14.Rq Other electron diffraction and scattering techniques for structure analysis – 61.72.Mm Grain and twin boundary

1 Introduction

The technique of Electron Backscatter Diffraction (EBSD) in a scanning electron microscope (SEM) was initially developed in the 1970's [1] when EBSD patterns were viewed on photographic film placed inside the microscope chamber. Improvements were made in the 1980's with the implementation of real-time imaging of EBSD patterns using a Silicon Intensified Target (SIT) low-light TV camera and phosphor screen which improved resolution and allowed lower probe currents to be used [2]. The next major step in the development of EBSD was the design of systems with fully automated pattern recognition and indexing procedures which allowed the rapid collection of orientation data from submicron regions (< 0.5 μm) of bulk specimens with an accuracy of approximately 1° [3,4]. In recent years, the automatic collection and analysis of EBSD patterns has been combined with automatic beam or stage control in the microscope to give a state-of-the-art system for plotting orientations, *via* colour coding, according to coordinates on the specimen. This technique is known as Crystal Orientation Mapping (COM) [5] or Orientation Imaging Microscopy (OIM) [6] and provides a dynamic visual representation of the morphological and orientational aspects of a microstructure in the form of a colour two-dimensional map.

[a] e-mail: r.k.davies@swansea.ac.uk

COM is becoming a popular technique for visualising the orientation distribution in the microstructure. As a result, the technique has been used in a wide range of applications involving a large variety of materials. Examples of several applications using COM are listed below:

- a study of the spatial arrangement of crystal orientations in as-cast and 40% channel die compressed aluminium [7];
- characterisation of cracked interfaces in a stress corrosion cracked nickel alloy and misorientation distributions in annealed high-purity copper plate [8];
- characterisation of interfaces in a hot-rolled Fe-1%Si alloy [9];
- orientation mapping of a polycrystal having two-phases, *i.e.* α-2Ti_3Al and γ-TiAl [10];
- *in situ* observations of deformation mechanisms in a recrystallised Al-5%Mg alloy [11];
- investigation and characterisation of "intra-grain" misorientations in recrystallised pure nickel [12].

The majority of investigations based on characterisation of deformation behaviour (the last two examples above) have traditionally been carried out using transmission electron microscopy (TEM) *e.g.* [13]. However, while having the advantage of being able to view directly the deformed substructure they are restricted to small volumes of crystal which in turn provides relatively poor statistics.

Recent investigations on both polycrystalline nickel [12] and aluminium [14] have shown that EBSD, used in line scan mode, can be used as an alternative to TEM for studying local lattice perturbations in the vicinity of grain boundaries and triple junctions. The reliability and efficiency of this technique has provided the impetus for extending this approach to applying COM to the study of local lattice orientations.

Most of the appeal of COM is in its visualisation aspects. However, without *quantification* and extraction of the pertinent information the COM is only of value as a depiction. In order to exploit the real benefits of COM, it is necessary initially to set up optimal microscopic acquisition parameters to obtain a suitable COM for the particular inquiry, and subsequently to apply suitable post-processing steps to extract quantitative data. The purpose of this paper is to show the quantitative application of COM for the case of deformation behaviour. The example chosen is the characterisation of local orientation perturbations near to triple junctions in an Al-3wt%Mg alloy deformed 5% in tension. First, the hardware configuration of the EBSD system (Sect. 2.1) and the microscope variables for EBSD are briefly described (Sect. 2.2). Measurements are made to determine the typical spatial resolutions of EBSD patterns that can be obtained with a Peltier-cooled charge coupled device (CCD) camera. This information is necessary in order to know the appropriate microscope conditions to select for the COM. For this purpose, measurements are performed on both pure aluminium and nickel specimens. A COM and pattern quality map of a triple junction are presented and finally the different methods of obtaining orientation perturbation data from the map are discussed and evaluated (Sect. 3).

2 Crystal orientation mapping – Experimental considerations

2.1 Hardware configuration

Investigative work was performed using the Link Opal EBSD system manufactured by Oxford Instruments and was interfaced to a JEOL 6100C SEM. The COM hardware configuration is shown in Figure 1. The basic features of this system are:

- a microscope interface kit which includes a phosphor screen, lead glass window and 70° tilted specimen holder;
- a Peltier-cooled CCD low-light TV camera and camera control unit for the integration of EBSD patterns. This camera has a high linearity so patterns appear less distorted when viewed on the phosphor screen. In addition, cooling reduces thermal noise in the CCD and allows the pattern to integrate on the CCD before being read out at TV rate at the end of the integration period. Integration times ranging between 40 ms and 100 s can be obtained which enables the use of a wide range of microscope operating conditions;

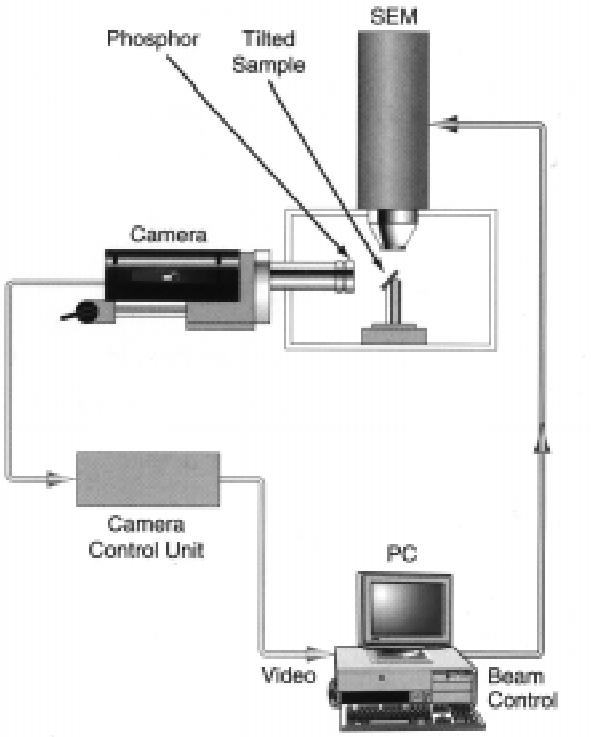

Fig. 1. Hardware configuration of the Link Opal EBSD system (courtesy of Oxford instruments).

- a 512×512 pixel $\times$ 8 bit PCI based framegrabber card and Pentium 150 MHz computer which is capable of processing an EBSD pattern in less than one second for medium atomic number elements at 20 kV;
- a forward mounted back-scattered electron detector which is placed in an optimum position to collect forward scattered electrons thus providing improved image acquisition during EBSD. This proves particularly useful when working with aluminium, since microstructural detail such as grain boundaries, shear bands etc. are not resolved using secondary electrons in the SEM because of the specific surface preparation requirements for EBSD [15].

2.2 Microscope operating conditions

The microscope variables to be considered when performing EBSD to construct a COM are:

- specimen tilt;
- working distance;
- probe current;
- accelerating voltage.

In normal operation the first two of these are fixed by geometrical considerations. The probe current is chosen mainly in accordance with the light sensitivity of the camera and the imaging requirements, since it has only a small effect on the spatial resolution of the probe [16,17]. A constant probe current of 2 nA was selected for the present

work. Accelerating voltage, on the other hand, is the major factor controlling spatial resolution with low accelerating voltages giving the best resolution. However, lowering accelerating voltage not only gives a reduced signal-to-noise ratio in the diffraction pattern but also progressively dims the pattern since the efficiency of the phosphor screen concurrently reduces, and automatic pattern recognition becomes more difficult.

The choice of spacing between the sampling points, *i.e.* the grid size, is under operator control when selecting set-up conditions for a COM. For the case considered here, a fine scale COM showing a lot of orientation perturbation detail over a small area, we need to select a spatial resolution which approaches the limit for a standard tungsten SEM. However, since smallest resolutions (achieved by low accelerating voltage) result in degraded diffraction patterns much longer integration times are required to achieve acceptable patterns which in turn increases the total map acquisition time and may also result in specimen contamination or drift. Hence, a suitable compromise is required between the accelerating voltage and the integration time. These effects were investigated in some detail as follows.

The spatial resolution of EBSD patterns was measured in pure aluminum and nickel specimens at accelerating voltages ranging between 10 kV and 20 kV. A tungsten filament was used in the SEM and the probe current and specimen working distance were kept constant at 2 nA and 19.5 mm respectively. The electron beam was moved digitally across a selected grain boundary and the distance between two clearly visible EBSD patterns was measured precisely from the beam coordinates. Measurements were taken in directions both parallel and perpendicular to the specimen tilt axis and the average spatial resolution was determined from a minimum of ten line scans.

The spatial resolutions measured in the aluminium and nickel specimens are shown in Figures 2a and 2b respectively. It is apparent from both graphs that resolution is very anisotropic due to interaction of the electron beam with a specimen which is tilted to 70°. A smaller spatial resolution is obtained in the direction parallel to the specimen tilt axis than that obtained in the direction perpendicular to the tilt axis. For aluminium (parallel to the tilt axis), a spatial resolution of 0.51 μm was obtained at 20 kV with a CCD camera integration time of 640 ms, which was considered to be acceptable for mapping. At lower accelerating voltages the resolution improved but this was accompanied by a reduction in the signal-to-noise ratio of the EBSD pattern and an increase in the pattern integration time (10 s at 10 kV). Working at accelerating voltages lower than 15 kV was found to be impractical since the long pattern integration times caused surface contamination, which in turn, degraded the pattern quality and prevented further measurements from being performed. Taking all these factors into consideration, it was decided that 20 kV accelerating voltage was optimum for mapping.

For nickel (Fig. 2b), spatial resolutions of 0.42 μm and 0.15 μm were obtained at 20 kV and 10 kV respectively with pattern integration times of 320 ms and 2.6 s. The results show very good agreement with previous resolution work performed on nickel using a similar EBSD system with a Peltier-cooled CCD camera [18]. In comparison to aluminium, shorter pattern integration times and smaller spatial resolutions are obtained in nickel under the same operating conditions. This would be expected with a higher atomic number element such as nickel.

Further improvement in spatial resolution is possible using a SEM equipped with a field emission gun (FEG). The high brightness of the FEG enables the beam diameter to be reduced in size at currents in the range of 10^{-9} A to 10^{-7} A which allows EBSD patterns to be obtained from smaller areas of the microstructure compared with that of a thermionic gun. The comparable spatial resolutions obtained from both a tungsten and LaB_6 filament in a (FEG) SEM have been reported as $\sim$ 200 nm and 50 nm at 10^{-8} A and $\sim$ 80 nm and 20 nm at 10^{-9} A respectively [19]. Furthermore, a study performed on a (100) Ni single crystal revealed that sub-grain boundaries with misorientations of 0.5° could be observed at a spatial resolution of < 20 nm $\times$ 80 nm [20].

More recently, resolution experiments performed in a (FEG) SEM using aluminium and platinum polycrystalline films showed that, whereas grains of $\sim$ 40 nm in diameter could be delineated occasionally in the aluminium sample, grains of 20 nm in diameter were normally resolved in the platinum sample [21].

2.3 Map acquisition

The image anisotropy caused by the 70° inclination of the specimen in the microscope chamber can be overcome by using a tilt correction facility during acquisition, which stretches the electron beam in the microscope Y direction so that the area sampled is the same as that in the microscope X direction. A square grid can then be superimposed on the captured image and the appropriate grid size selected. The electron beam is programmed to move digitally to each grid point where it acquires an EBSD pattern which is viewed on the phosphor screen. The pattern is integrated in real-time prior to background subtraction which improves the signal-to-noise ratio.

The Link Opal software uses automatic pattern recognition to detect the position of Kikuchi bands in the EBSD pattern. The algorithm used for solving patterns is based on the Hough transform [22] which provides a method for deriving the parameters of a straight line and is governed by the equation $p = x\cos 0 + y\sin 0$. This relationship transforms all (x, y) points on the same straight line to sinusoidal curves in $(p, 0)$ Hough space. The lines corresponding to the strongest peaks are detected and then all possible combinations of line intersections are compared to the known crystal symmetry of the material. The derived crystallographic orientations are then stored as a 3×3 orientation matrices.

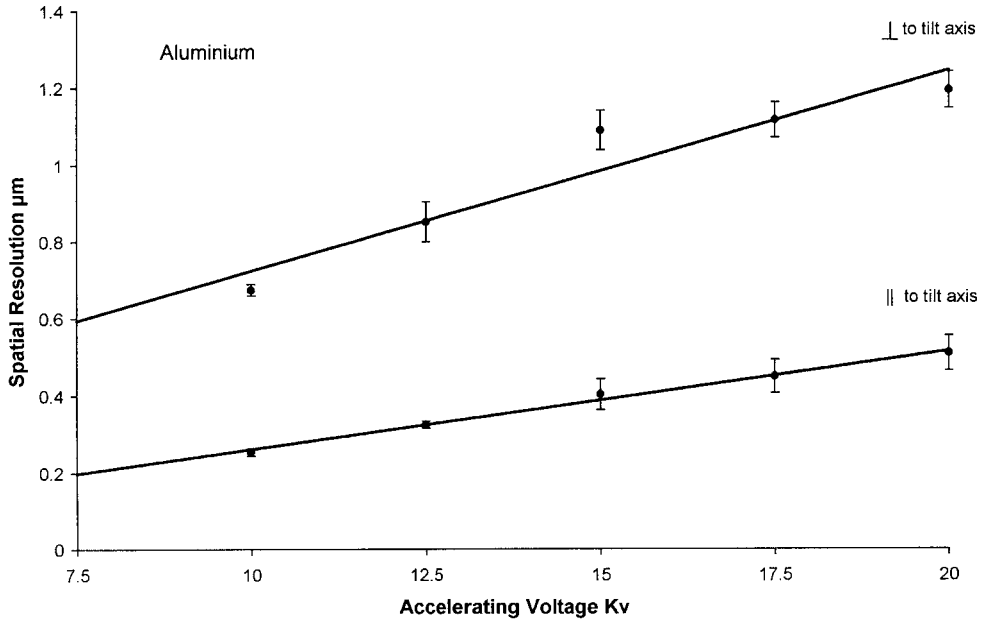

(a)

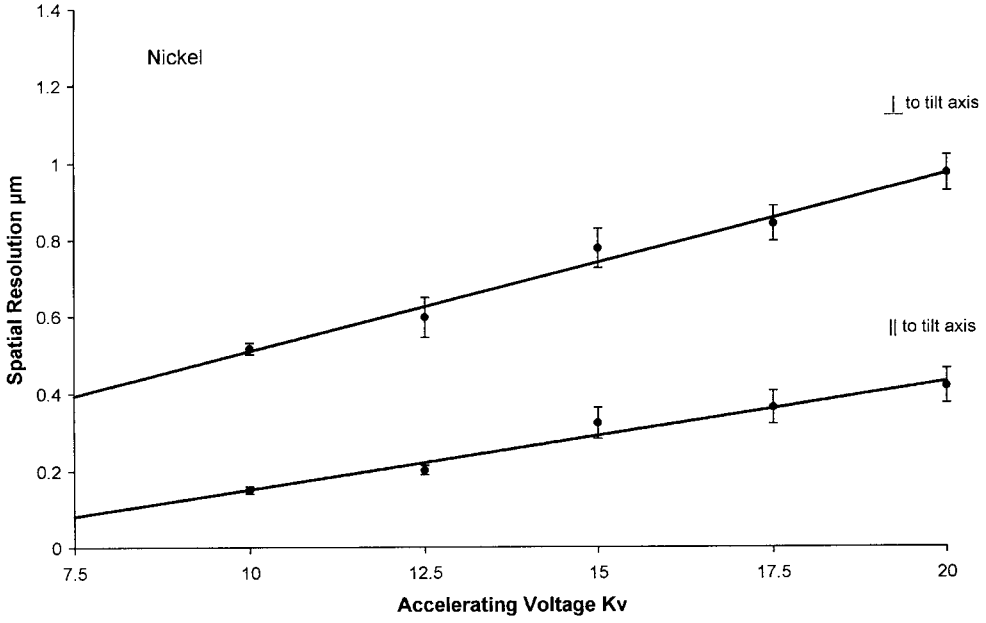

(b)

Fig. 2. Spatial resolution of EBSD patterns measured in (a) aluminium and (b) nickel, as a function of accelerating voltage.

Table 1. Composition (wt%) of the Al-Mg alloy used in the present investigation.

Mg	Si	Fe	Cu	Mn	Zn	Ti	B
2.99	0.005	< 0.01	0.001	< 0.001	< 0.001	< 0.001	< 0.001

3 Application of COM to local orientation measurements

3.1 Data collection

COMs were generated in the vicinity of triple junctions in a binary Al-3wt%Mg alloy supplied by Alcan International Limited, the composition of which is given in Table 1. The ingot was homogenised at 500 °C and hot rolled to a 50% reduction in thickness (25 mm to 12.5 mm gauge). The slab was then annealed for one hour at a temperature of 350 °C to obtain an equiaxed grain size of approximately 150 μm. Specimens were then deformed 5% in tension which resulted in an average grain size of 200 μm. In the present study, a tensile strain was applied to specimens in preference to cold rolling so that a homogeneous strain distribution is produced through the sheet thickness, a feature which is very difficult to achieve at low cold reductions (5%).

Specimens for analysis were ground using standard metallographic procedures and then electropolished using an electrolyte of 5% perchloric acid in ethanol for two minutes using 40 volts at a temperature of −20 °C. An image of the triple junction was acquired *via* the forward mounted back-scattered electron detector and a square grid of 1 μm was selected for mapping. From the discussion in the previous section it was shown that at an accelerating voltage of 20 kV, a spatial resolution of 0.5 μm can be obtained together with a high pattern signal-to-noise ratio. Therefore, the selected grid size of 1 μm is well within the limit of spatial resolution. Each COM was built-up in real time and comprised 704 data points which were aligned in rows, resulting in map acquisition time of 19 min. Each square pixel was designated a colour depending on its crystallographic orientation, *i.e.* red, blue and green are assigned to the 001, 111 and 101 directions respectively in the inverse pole figure.

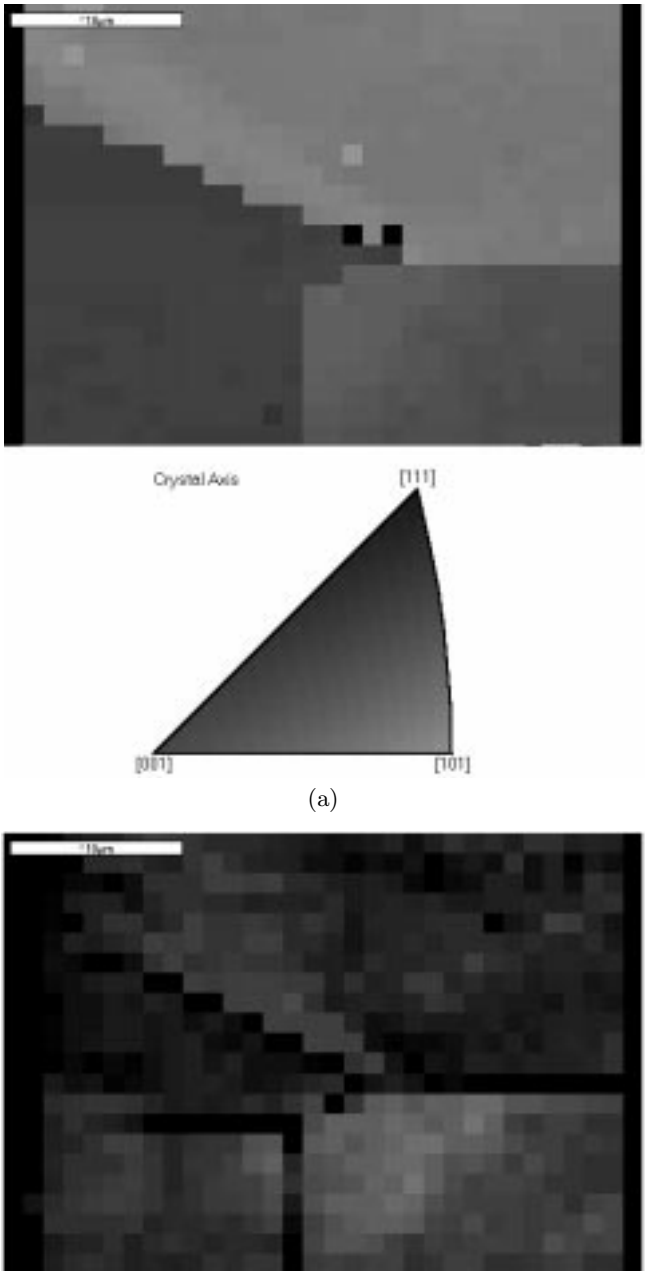

(a)

(b)

Fig. 3. (a) Crystal orientation map and (b) pattern quality map of a triple junction in an Al-3wt%Mg alloy deformed 5% in tension.

3.2 Data representation

The orientation data generated from COMs were used to quantify local orientation perturbations in the vicinity of triple junctions. Such data can be represented in several different ways. The method of each is discussed below and is applied to orientations from the same data set for comparison.

3.2.1 Crystal orientation maps

An example of a crystal orientation map of the specimen normal direction in the vicinity of a triple junction is shown in Figure 3a. In the bottom right hand grain a change in orientation can be seen as the triple junction is approached. There are also several pixels at the junction which are black. These depict EBSD patterns which were not solved which, in the present case, is due to the high concentration of localised strain at the triple junction which degrades pattern quality. Alternatively, the orientation data can be represented as a pattern quality map as shown in Figure 3b. This is constructed from a pattern quality index value (Q) which is calculated from the sum of the heights of the detected peaks in Hough space [22]. The dark colour pixels (high Q value) are located along the grain boundaries and represent EBSD patterns which are poor in quality. The pattern quality map, therefore, gives an indication of the distribution of strain in the vicinity of the triple junction.

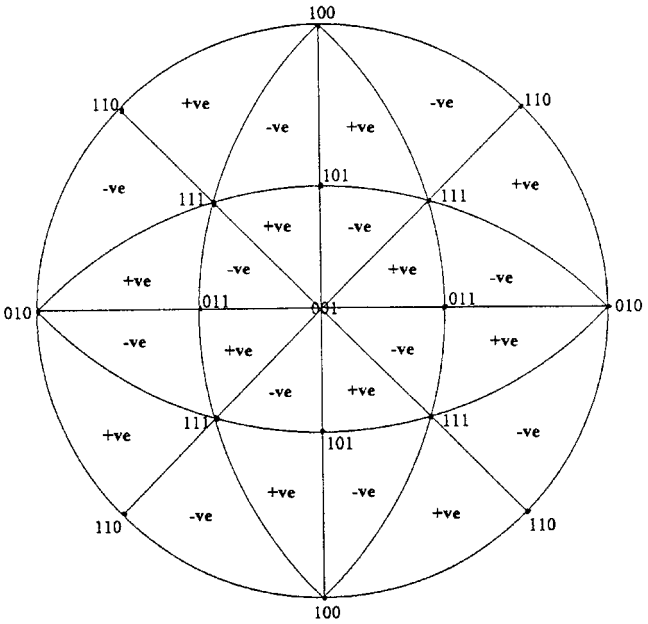

Fig. 4. Schematic diagram of the (001) stereographic projection used to calculate the sense of the misorientation angle (θ). θ is taken to be positive if the misorientation axis $[hkl]$ lies in the right-hand unit triangle and θ is taken to be negative if $[hkl]$ lies in the left-hand unit triangle of the stereographic projection.

Although the COM in Figure 3a provides a two-dimensional visual representation of local orientation perturbations it only serves as a qualitative measure. In order to quantify orientation perturbations it is necessary to represent the data in a different format. This was achieved by extracting the orientation matrices or "raw data" stored with the COM and employing post-processing steps using in-house software. To illustrate the different methods available for representing local orientation perturbations, orientation data were extracted from the line marked in Figure 3a.

3.2.2 Misorientations between contiguous sampling points

During mapping the EBSD pattern from each sampling point can be viewed in real-time as the COM is being built-up. The EBSD patterns collected in the present experiments were observed to rotate discretely between an anti-clockwise and clockwise direction as the electron beam traversed the specimen, which implies that the misorientations are not cumulative in manner. Furthermore, in order to obtain information about the spatial orientation changes that occur within a subdivided grain, the sense of the misorientation angle (θ) was calculated based on the position of the misorientation axis ($[hkl]$) in the stereographic projection. θ is taken to be positive if $[hkl]$ lies in the right-hand unit triangle of the stereographic projection and θ is taken to be negative if $[hkl]$ lies in the left-hand unit triangle as illustrated in Figure 4.

The misorientation between contiguous sampling points plotted as a function of sampling distance is shown in Figure 5a. In order to highlight the importance of the *sense* of the misorientation, the data has been plotted both with and without the sign represented by a broken line and bold line respectively. In the left hand grain there is no variation in misorientation. An error band of $\pm 0.5°$ is adopted for misorientation measurements and therefore a lattice rotation or orientation perturbation is considered to be in excess of 0.5°. The right hand grain, however, exhibits orientation perturbations of up to about 5° which are periodic in manner. The disadvantage of this method is that the size of the misorientations depends on the sampling step size used. In addition, both the angle and axis have to be inspected simultaneously to obtain information on the misorientation distribution since inspection of only one plot can be very misleading [14].

3.2.3 Angular distance in Euler space

An alternative method of expressing the data above is to plot the angular distance between each sampling point and a reference point (representative of the average grain orientation) in Euler space. The three orientation parameters are compressed into a single variable known as the Euler parameter D_{E}. In the present case, the reference point was taken to be the sampling point furthest away from the grain boundary. The angular distance in Euler space was calculated using the following equation [23]

$$D_{\mathrm{E}} = [(\varphi_1 - \langle\varphi_1\rangle)^2 + (\Phi - \langle\Phi\rangle)^2 + (\varphi_2 - \langle\varphi_2\rangle)^2]^{1/2}$$

where φ_1, Φ, φ_2 are the Euler angles of the sampling points and $\langle\varphi_1\rangle$, $\langle\Phi\rangle$, $\langle\varphi_2\rangle$ are the Euler angles of the reference point.

The disadvantage of using this method of representation is that due to the non-linearity of Euler space and the fact that Euler angles are correlated, misleading values of D_{E} may be obtained. Secondly, with such a single parameter method occasionally different orientations are represented by the same D_{E} parameter. However, the problem of the non-linearity of Euler space can be taken into account by using a modified equation [24]

$$D_{\mathrm{EC}} = [(\varphi_1 - \langle\varphi_1\rangle)^2 + (\Phi - \langle\Phi\rangle)^2 + (\varphi_2 - \langle\varphi_2\rangle)^2 - 2\cos\Phi(\varphi_1 - \langle\varphi_1\rangle)(\varphi_2 - \langle\varphi_2\rangle)]^{1/2}.$$

Figure 5b shows the angular distance in Euler space D_{E} (bold line) and corrected angular distance in Euler space D_{EC} (broken line) as a function of sampling distance. A large orientation perturbation is observed adjacent to the boundary of the right hand grain, the magnitude of which is smaller when plotted using the corrected parameter D_{EC}. Grain boundaries comprising such large orientation perturbations have been defined as "boundary zones" [14], *i.e.* having a D_{E} parameter greater than approximately 1.5 times than that within the grain. Previous work has also proved that orientation data can be represented equivalently by plotting the angular distance in Rodrigues-Frank (RF) space [14].

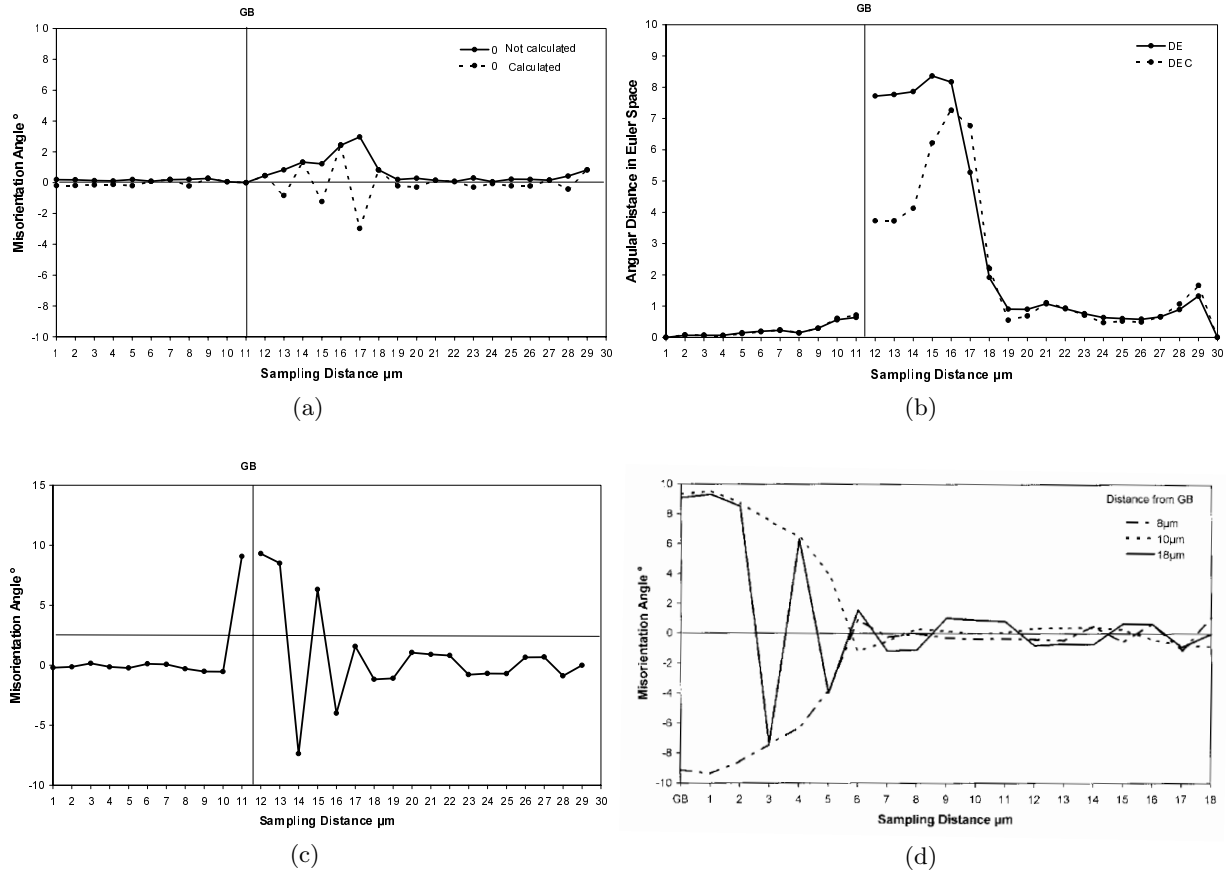

Fig. 5. (a) Orientation perturbation data represented as misorientations measured between contiguous sampling points (method (ii)). (b) Orientation perturbation data represented as the angular distance in Euler space using both non-corrected (D_{E}) and corrected (D_{EC}) Euler parameters (method (iii)). (c) Pattern of orientation perturbation observed when misorientations are measured between each sampling point and a reference point (method (iv)). (d) Variation in the pattern of orientation perturbation observed when misorientations are measured relative to different reference points, *i.e.* at sampling distances of 8 μm, 10 μm and 18 μm from the grain boundary respectively.

3.2.4 Misorientations relative to a reference point

Using the same data set, the misorientation angle was measured between each sampling point and a reference point which was taken to be the sampling point furthest away from the grain boundary, *i.e.* the average orientation of the grain. The pattern of orientation perturbation as a function of sampling distance is shown in Figure 5c. The left hand grain shows no orientation perturbations within the grain but directly adjacent to the grain boundary there is an orientation difference of approximately 9°. The right hand grain exhibits large perturbations in excess of 15° at the grain boundary which extends 5 μm into the grain. The perturbations alternate with a positive and negative sign and have a periodicity of about 1 μm.

This method of data representation has the advantage that the magnitude of the misorientations does not depend on the sampling step size, however, the size of the misorientations are dependent on the selection of the reference point. This must be given some careful consideration as an inappropriate selected reference point can bias the whole data set. This point is exemplified in Figure 5d where lattice misorientations belonging to the same data set have been plotted using different selected reference points, *i.e.* distances of 8 μm (i), 10 μm (ii) and 18 μm (iii) away from the grain boundary respectively. All three curves show large misorientation differences (10°–15°) in the grain boundary region and small differences in the grain interior. However, the misorientations are periodic in nature when reference point (iii) is selected and are accumulative when reference points (i) and (ii) are chosen.

3.2.5 Summary

Orientation perturbation data extracted from the COM has been represented using three different data processing methods. Method (ii) has the disadvantage that the size of the misorientation is dependent on the sampling step size used. In addition, since misorientations are measured between neighbouring sampling points and not relative to a reference point (*i.e.* the point furthest away from the grain boundary), any large orientation perturbations which may be present at the grain boundary are not displayed.

This is illustrated in Figure 5a where a misorientation of approximately 2.5° is observed at the boundary, significantly smaller than would be expected.

In comparison, method (iii) measures the angular distance in Euler space relative to the average orientation of the grain which enables long-range variations in orientation, *i.e.* between the grain interior and grain boundary to be represented (Fig. 5b). However, in addition to the problems outlined, this method is disfavoured by the fact that it is not possible to calculate the sense of the angular distance in Euler space.

Method (iv) has the disadvantage that the size of misorientations depends on the selection of the reference point and if inappropriately chosen, can bias the whole data set giving a misleading representation. However, as with method (iii), the reference point is taken as the average grain orientation which enables local orientation perturbations at the grain boundary to be quantified relative to the grain interior. In addition, the sense of misorientation can be calculated using this method. This is shown in Figure 5c where orientation perturbations are periodic in manner and have a magnitude of approximately 18° in the grain boundary region which would be expected in such regions containing high levels of localised strain. Thus, for the reasons above, this method is considered to be the optimum method for quantifying local orientation perturbations in the vicinity of triple junctions in this particular investigation.

4 Concluding remarks

The hardware configuration of a state-of-the-art Crystal Orientation Mapping (COM) system for making spatially specific orientation measurements has been described. The spatial resolution of EBSD patterns has been measured in pure aluminium and nickel specimens and COM has been used to characterise local orientation perturbations in the vicinity of triple junctions in an Al-3wt%Mg alloy deformed 5% in tension. The main conclusions from this work are:

1. smaller spatial resolutions are favoured with lower accelerating voltages but this is accompanied with reduced pattern signal-to-noise ratios resulting in longer pattern integration times. For aluminium, spatial resolutions of 0.25 μm and 0.51 μm were measured at accelerating voltages of 10 kV and 20 kV respectively. The spatial resolutions for nickel measured at the same voltages were 0.15 μm and 0.42 μm respectively;
2. COM is a very powerful tool for studying local orientation perturbations and hence deformation structures. It provides a dynamic visual representation of the morphological and orientational aspects of a microstructure in the form of a colour two-dimensional map. However, for maximum benefit in an investigation the visual appreciation of a COM must be coupled with extraction of quantified data;
3. data has been extracted from a COM and represented in the form of (a) misorientations between contiguous sampling points, (b) angular distance in Euler space and (c) misorientations relative to a reference point. Method (c) proved to be the optimum method for data representation because it allowed the quantification of local orientation perturbations at the grain boundary relative to the grain interior. Also, the sense of the misorientation is calculated which provides information about the spatial orientation changes within the grain.

R.K. Davies is grateful to EPSRC for their financial support and to the Risø National Laboratory and Alcan International Limited for providing the specimens.

References

1. J.A. Venables, C.J. Harland, Philos. Mag. **27**, 1193 (1973).
2. D.J. Dingley, Scan. Elec. Micro. **4**, 273 (1981).
3. D. Juul Jensen, N.H. Schmidt, in *Proceedings of Recrystallisation'90*, Ohio, 1990, edited by T. Chandra, p. 219.
4. N.H. Schmidt, J.B. Bilde-Soresen, D. Juul Jensen, Scan. Micro. **5**, 637 (1991).
5. V. Randle, S.H. Vale, Materials World **5**, 574 (1997).
6. S.I. Wright, J. Comp. Ass. Micro. **5**, 212 (1993).
7. S.I. Wright, B.L. Adams, K. Kunze, Mat. Sci. Eng. A **160**, 229 (1993).
8. T.A. Mason, B.L. Adams, J. Metals **46**, 43 (1994).
9. B.L. Adams, S.I. Wright, K. Kunze, Met. Trans. A **24**, 819 (1993).
10. S.I. Wright, D.P. Field, in *Proceedings of Microscopy and Microanalysis'97*, Cleveland, Ohio, 1997, edited by G.W. Baily, R.V.W. Dimlich, K.B. Alexander, J.J. McCarthy, T.P. Pretlow, p. 561.
11. H. Weiland, in *Proceedings of Microscopy and Microanalysis'97*, Cleveland, Ohio, 1997, edited by G.W. Baily, R.V.W. Dimlich, K.B. Alexander, J.J. McCarthy, T.P. Pretlow, p. 563.
12. V. Randle, R.K. Davies, Philos. Mag. A (submitted).
13. C.Y.J. Barlow, B. Bay, N. Hansen, Philos. Mag. A **51**, 253 (1985).
14. V. Randle, N. Hansen, D. Juul Jensen, Philos. Mag. A **73**, 265 (1996).
15. R.K. Davies, V. Randle, Mat. Char. **37**, 131 (1996).
16. J. Hjelen, E. Nes, in *Proceedings of the XII International Congress for Electron Microscopy*, Japan, 1990, p. 404.
17. J. Hjelen, A.H. Quale, Ø. Gomo, Mat. Sci. For. **157-162**, 137 (1994).
18. A. Drake, S.H. Vale, in *the Proceedings of EMAG 95*, Birmingham, 1995, p. 137.
19. J.A. Venables, A.P. Janssen, Ultramicroscopy **5**, 297 (1980)
20. C.J. Harland, P. Akhter, J.A. Venables, J. Phys. E: Sci. Instrum. **14**, 175.
21. D.J. Dingley, D.P. Field, in *the Proceedings of 5th Workshop on EBSD*, University of Oxford, Royal Microscopical Society, 1998, p. 4.
22. N.C. Krieger Lassen, D. Juul Jensen, K. Conradsen, Scan. Micro. **6**, 115 (1992).
23. N. Hansen, D. Juul Jensen, Mat. Sci. For. **157-162**, 1211 (1994).
24. D. Juul Jensen (private comminication).